Carrier Synchronization Method using High-Speed Sampling for Parallel Inverters without Communication

Takumi Iwamoto, Hiroki Watanabe, Yuki Nakata and Jun-ichi Itoh
NAGAOKA UNIVERSITY OF TECHNOLOGY
1603-1, Kamitomioka-machi, Nagaoka, Niigata, Japan
Tel.: +81 / (258) – 47.9533.
E-Mail: s225057@stn.nagaoaut.ac.jp, hwatanabe@vos.nagaokaut.ac.jp, ynakata@vos.nagaokaut.ac.jp, itoh@vos.nagaokaut.ac.jp
URL: http://itohserver01.nagaokaut.ac.jp/itohlab/jp/index.html

Acknowledgements

This work was supported by the Council for Science, Technology and Innovation(CSTI), the Cross-ministerial Strategic Innovation Promotion Program (SIP), and the 3rd period of SIP " Smart energy management system " Grant Number JPJ012207 (Funding agency:JST).

Keywords

«Parallel operation», «Inverter», «Single-phase system», «Synchronization», «High-speed sampling».

Abstract

This paper proposes a novel carrier-synchronized control method for the parallel operation of two inverters using high-speed sampling. The proposed method focuses on the active power component at the switching frequency. When carrier synchronization is achieved, the active power at the switching frequency becomes zero for inverters connected in parallel. The proposed method calculates the active power at the switching frequency using high-speed sampling, switching states, and the fast Fourier transform (FFT). The proposed method requires only DC voltage and inductor current measurement without additional sensors. Furthermore, the proposed method is implemented in a single-phase inverter and does not need communication between units. Experimental results demonstrate that the circulating current is successfully suppressed to less than 66% of the rated current, thereby, validating the efficacy of the proposed control method.

Introduction

In recent years, renewable energy applications and electric vehicles have been promoted from the perspective of achieving carbon neutrality. Accordingly, the application range of power converters has expanded, and elemental technologies such as circuit topology, control methods, and design methods have been developed for each application [1-3]. The development of power converters requires specialized and multifaceted expertise, including circuit design, software development, and thermal management, which in turn results in significant time and cost requirements. In order to accommodate a wide range of demands for power converters in the future, it is important to develop a power conversion system rapidly and cost-effectively.

One approach under consideration to reduce development time is the use of modular structures, such as a Power Electronics Building Block (PEBB) [4-5]. The PEBB concept enables the realization of a power conversion system by combining multiple modules, each of which is optimized for high power density. Since the main circuit design is already included in the module, the overall development time can be significantly shortened. Moreover, maintenance is simplified, as faulty modules can be easily replaced. However, while the main circuit and certain auxiliary circuits can be modularized, the controller and detection circuits still need to be developed separately, which adds time and cost to the process.

Fig. 1 shows the configuration of a power conversion system using Universal Smart Power Module (USPM) concept. The USPM has been proposed to further reduce the development times and reduce costs within the PEBB concept [6-8]. The USPM modularizes all components of the

power converter, including not only the main power circuit but also the controller and detection circuits. By simply selecting and combining USPMs, a power conversion system can be quickly designed, thus greatly reducing the development time. In this configuration, each USPM performs a specific role, and a master controller manages the overall system. The USPM has high-speed controller and responds quickly to commands from the master controller to achieve power conversion. Furthermore, the USPM can be connected in series and parallel, enabling their applications to high-voltage and high-current systems. However, circulating currents caused by carrier asynchrony in parallel connected autonomous power converters, such as the power conversion system using USPM. Therefore, carrier synchronization is necessary.

The conventional carrier synchronization method [9] requires a signal line to the master controller or the other converter. On the other hand, the USPM system relies on wireless communication, which is slower and less reliable, between the master controller and each USPM. Therefore, the USPM systems require carrier synchronization that does not require communication with the master controller or other USPMs. The carrier synchronization methods without communication have been proposed in [10] and [11]. While these methods remove the dependency on signal transmission, their robustness against noise and external disturbances remains a significant concern, potentially limiting their practical applicability in noisy operating environments.

This paper proposes a carrier-synchronized control method for two inverters connected in parallel using high-speed sampling. The new contribution of this paper is the establishment of a carrier synchronization method that is resistant to noise and does not require high-speed communication with other converters or controllers. As a result, the circulating current is suppressed by carrier synchronization of the inverters. The proposed method synchronizes the carrier by focusing on the active power of the switching frequency component being zero when the carrier phase difference is 0°. In particular, the active power of the switching frequency component is calculated using high-speed sampling and Fast Fourier Transform (FFT), and the carrier phase is shifted so that the active power is zero. The proposed method uses FFT and integral calculation to effectively minimize the impact of noise. The rest of this paper is organized as follows: first, the circulating current in the parallel connection of a single-phase inverter is derived; next, the proposed carrier synchronization method is explained; finally, the effectiveness of the control method is verified through the verification of the simulation and the experiment.

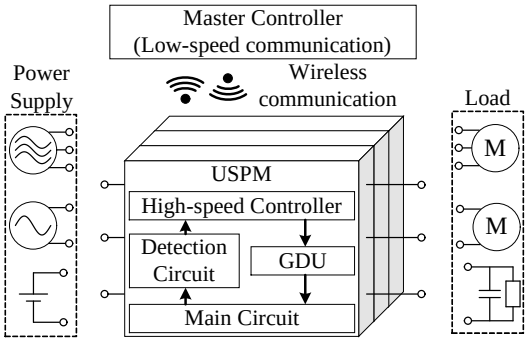

Fig. 1. Power conversion system using USPM. Each USPM operates autonomously, and communication between USPMs is via a master controller.

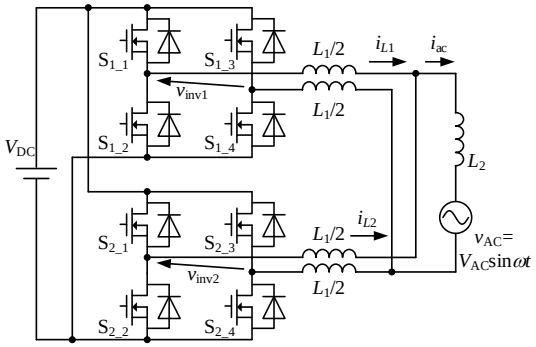

Fig. 2. Single-phase inverter with two units connected in parallel. ω is the angular frequency of the grid.

Circuit configuration and derivation of circulating current

Fig. 2 shows the circuit diagram of two inverters connected in parallel. This circuit is assumed to be grid-connected. The two inverters operate with bipolar modulation, and each inverter has its own current controller. The current command value is transmitted from the master controller and operates at the same value. Circulating currents due to carrier asynchrony are a common issue in autonomous distributed power converters. In this paper, for simplicity, the circulating current is derived from the

fundamental component of the switching frequency.

Fig. 3 shows the equivalent circuit at the fundamental component of the carrier. ω_{sw} is the angular frequency of the switching frequency component and δ is the phase difference of the carrier between two inverters. The currents i_1 and i_2 flowing through in each inverter are given by

$$i_1 = \frac{L_1 + L_2}{\omega_{sw}\left(L_1^{\,2} + 2L_1L_2\right)} V_{\mathrm{DC}} \sin\left(\omega_{sw}t - \frac{\pi}{2}\right) - \frac{L_2}{\omega_{sw}\left(L_1^{\,2} + 2L_1L_2\right)} V_{\mathrm{DC}} \sin\left(\omega_{sw}t - \frac{\pi}{2} + \delta\right) \quad \text{.....(1),}$$

$$i_2 = -\frac{L_2}{\omega_{sw}\left(L_1^{\,2} + 2L_1L_2\right)} V_{\mathrm{DC}} \sin\left(\omega_{sw}t - \frac{\pi}{2}\right) + \frac{L_1 + L_2}{\omega_{sw}\left(L_1^{\,2} + 2L_1L_2\right)} V_{\mathrm{DC}} \sin\left(\omega_{sw}t - \frac{\pi}{2} + \delta\right) \quad \text{.....(2).}$$

The circulating current is given by i_1 and i_2 and by

$$i_1 - i_2 = 2\sin\left(-\frac{\delta}{2}\right) \frac{L_1 + 2L_2}{\omega_{sw}\left(L_1^{\,2} + 2L_1L_2\right)} V \sin\left(\omega_{sw} + \frac{\delta}{2}\right) \quad \text{.....(3).}$$

From (3), the amplitude of the circulating current contains a sine function with carrier phase difference δ. Therefore, the circulating current becomes zero when the carrier phase difference is zero.

Next, the relationship between active power and carrier phase difference is investigated. Equation (1) is simplified and is given by

$$i_1 = I_1 \sin\left(\omega_{sw}t - \phi\right) \quad \text{.....(4),}$$

where the amplitude I_1 and phase difference ϕ between the carrier frequency component of the inverter output voltage and the inductor current of i_1 are given by

$$I_1 = \frac{V_{\mathrm{DC}}}{\omega_{sw}\left(L_1^{\,2} + 2L_1L_2\right)} \sqrt{L_1^{\,2} + 2L_2\left(L_1 + L_2\right)\left(1 - \cos\delta\right)} \quad \text{.....(5),}$$

$$\phi = \arccos\left(\frac{-L_2 \sin\delta}{\sqrt{L_1^{\,2} + 2L_2\left(L_1 + L_2\right)\left(1 - \cos\delta\right)}}\right) \quad \text{.....(6).}$$

From (6), the current phase difference ϕ is 90° when the carrier phase difference δ is 0° or 180°. Also, the instantaneous power is given by

$$p_1 = \frac{1}{2} V_{DC} I_1 \left\{\cos\phi - \cos\left(2\omega_{sw}t + \phi\right)\right\} \quad \text{.....(7),}$$

where substituting ϕ=90°, the active power (average power) is zero. Thus, (6) and (7) show that during carrier synchronization, the power factor of the carrier frequency component is zero, and the active power is zero. Therefore, carrier synchronization is achieved by controlling the carrier phase angle of the inverter so that the active power is zero.

Fig. 4 shows the current phase and the active power versus the carrier phase difference. The

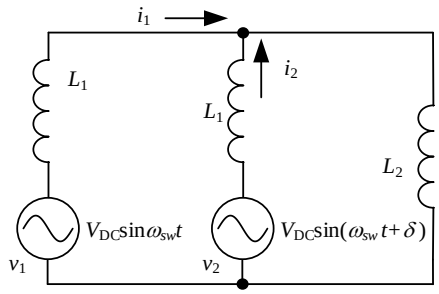

Fig. 3. Equivalent circuit of the carrier frequency components for a single-phase inverter with two units connected in parallel. i_1 and i_2 are the carrier frequency components of the inductor current, and δ is the carrier phase difference between v_1 and v_2.

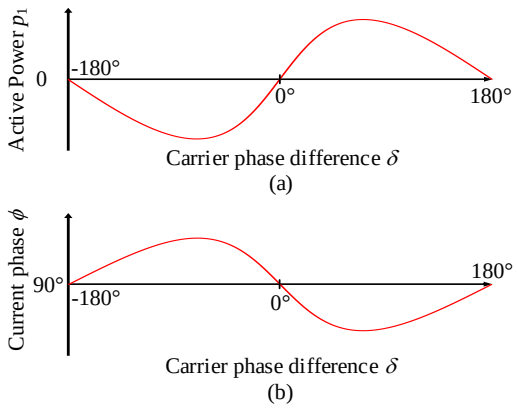

Fig. 4. Carrier phase difference versus current phase and active power. When the power supply v_1 is phase lag versus v_2 ($\delta > 0°$), the active power of v_1 is positive and the inductor current i_1 is phase lag by more than 90° versus v_1 ($\phi > 90°$). On the other hand, when v_1 is phase lag versus v_2 ($\delta < 0°$), the active power is negative and i_1 phase lag is less than 90° versus v_1 ($\phi < 90°$). (a) Active power. (b) Current phase.

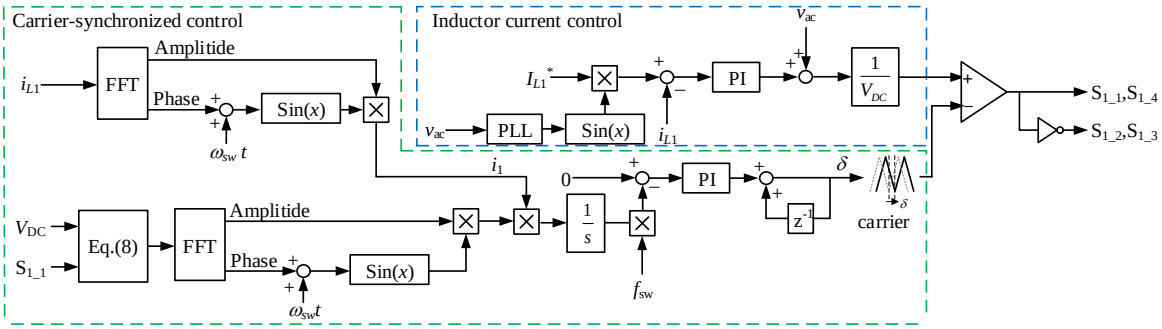

Fig. 5. Control block of proposed control. Inductor current control section is configured by PI control.

active power is zero when the carrier phase difference δ is 0° and 180°. Therefore, it is essential to consider the direction of the carrier phase shift. From Fig. 4, carrier synchronization is achieved by leading the carrier phase when the active power is positive and lagging the carrier phase when the active power is negative.

Carrier synchronization method

Fig. 5 shows the control block diagram of the proposed carrier synchronization method. The inductor current control section uses a PI controller to control the inverter current i_{L1} so that the power factor with the grid voltage is unity.

In the proposed carrier synchronous control, first, the amplitude and phase of the carrier frequency components are obtained from the high-speed sampled inductor current i_{L1} and inverter voltage v_{inv1} by FFT [12]. Next, the instantaneous power is calculated from the acquired amplitude and phase of the fundamental components i_1 and v_{inv1} and integrated. The active power is calculated from the product of the integral and the switching frequency. The calculation period of FFT and the active power should be an integer multiple of the carrier period in order to reduce quantization errors. Note that v_{inv1} is not detected and given from V_{DC} and the state of the switches by

$$\begin{cases} v_{inv1} = V_{DC} & (S_{1\_1} = 1) \\ v_{inv1} = -V_{DC} & (S_{1\_1} = 0) \end{cases} \quad \text{.....(8).}$$

The carrier phase difference is shifted by PI control so that the calculated active power is set to zero. The control period of the PI control depends on the active power calculation period.

This control uses only the switching state of the autonomous operated inverter and the detection of the input voltage V_{DC}, grid voltage v_{ac} and inductor current. Therefore, the proposed method does not require information from the other inverter and achieves carrier synchronization without communication with the master controller or other inverters. Detection noise is also a significant problem in high-speed sampling. However, the proposed control uses FFT calculation to obtain the switching frequency component of the inductor current. Therefore, the noise of the sampling frequency component is eliminated due to white noize.

Table 1 Simulation condition.

Quantity	Symbol	Value
DC voltage	V_{DC}	400 V
Grid voltage	v_{ac}	200 V_{rms}
Grid frequency	f	50 Hz
Rated current of one unit	i_{ac}	20 A_{rms}
Rated power of one unit	P_1,P_2	4 kW
Inverter side inductance	L_1	640 μH (%Z=2%)
Grid side inductance	L_2	320 μH (%Z=2%)
Switching frequency	f_{sw}	100 kHz

Simulation Verification

Table 1 shows the simulation conditions. In this paper, a USPM controller is assumed, and the inductor current is sampled at 10 MHz. FFT and the active power are performed in the range of 10 cycles of the switching frequency in order to reduce quantization error. In addition, the inductor current control operates in the switching cycle.

Fig. 6 shows the grid voltage, inductor current, the circulating current, the active power of the switching frequency component, and the carrier phase difference d during rated power operation in the simulation. The RMS value of the

circulating current before carrier synchronization is 410 mA (0.021p.u.), and that after synchronization is reduced to 32 mA (0.0016p.u.). This result clearly demonstrates that the circulating current is suppressed by the carrier synchronization. In addition, the circulating current before carrier synchronization contains a component that fluctuates at a period of the grid frequency of 50 Hz and a component that fluctuates at a carrier frequency of 100 kHz. The circulating current due to carrier asynchrony is affected by the duty cycle. In addition, the duty cycle varies with the grid voltage. Therefore, the circulating currents due to carrier asynchrony include the grid frequency component. In this paper, the carrier synchronization method focuses only on the circulating current of the carrier frequency component. However, the circulating current of the 50 Hz component is suppressed after carrier synchronization because the 50 Hz component is also caused by carrier asynchrony. In addition, the active power occurs before carrier synchronization. The active power is kept nearly zero by turning on carrier synchronization control. As a result, the carrier phase difference δ is also nearly 0°. The maximum phase difference after carrier synchronization is 1.4°.

Fig. 7 shows the inverter output voltage and inductor current before and after carrier synchronization. The initial phase difference of the inverter output voltage is set to 30°, and the inductor current is not a triangular wave before carrier synchronization. On the other hand, and the inductor current is a triangular wave after carrier synchronization. In addition, before carrier synchronization, a potential difference occurs due to the circulating current. This increases the current ripple and the current RMS value. On the other hand, after carrier synchronization, a potential difference does not occur because there is no circulating current. Therefore, only the load current flows, and the current RMS value decreases.

Fig. 8 shows the circulating currents versus sampling frequency and FFT calculation period. The circulating current remains nearly constant when the sampling frequency exceeds 20 times the switching frequency. Therefore, the sampling frequency should be set between 20 and 30 times the switching frequency. This adjustment allows the switching frequency to be set from 3 to 5 times higher compared to cases where the sampling frequency is set to 100 times the switching frequency. In addition, the quantization error is reduced by increasing the calculation period of

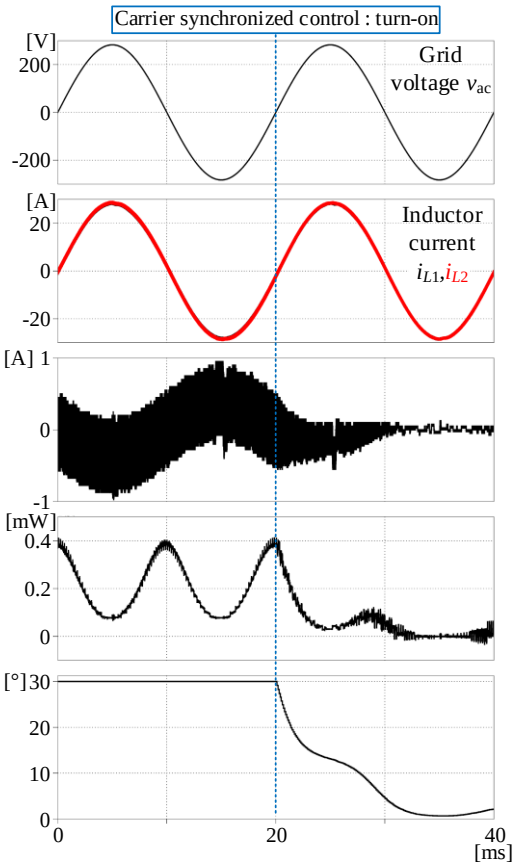

Fig. 6. The output voltage, the inductor current, the circulating current, the active power of switching frequency component, and the carrier phase difference. The carrier phase difference before carrier synchronization is set to 30°, and the carrier synchronization control is turned on in 20 ms.

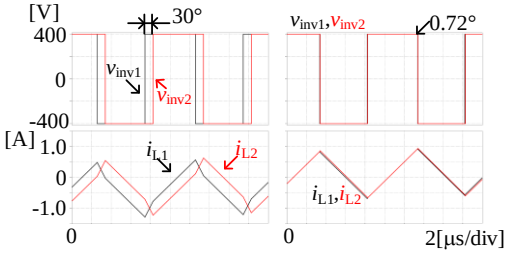

(a) (b)

Fig. 7. Magnified waveforms of inverter voltage and inductor current. The carrier phase difference before carrier synchronization is set to 30°. (a) Before carrier synchronization. (b) After carrier synchronization.

FFT. The circulating current is reduced to less than 0.0014p.u. (at 500 cycles FFT) when the

sampling frequency is 100 times the switching frequency.

Experimental verification

Table 2 shows the experimental conditions. In this experiment, low carrier frequency was used to verify the effect of the proposed method. In addition, the same controller is used in the two inverters to set the initial phase difference. Note that information is not shared between the two inverters. Besides, the current phase is compensated beforehand for the detection delay of the current sensor.

Fig. 9 shows the waveforms before and after carrier synchronization. Fig. 10(a) shows the waveforms before carrier synchronization. The initial phase difference δ is set to 15°. The circulating current has a DC component. The circulating current is evaluated in terms of the AC component, as the carrier synchronization method affects only the AC component of the circulating current. This is due to inverter detection errors and imbalance of the inductance values. The RMS value of the AC component in the circulating current before carrier synchronization is 740 mA. The circulating current is caused by the carrier phase difference. In addition, similar to the simulation results, the circulating current contains a component that fluctuates at a grid frequency of 50 Hz and a component that fluctuates at a carrier frequency of 10 kHz. In contrast, Fig. 10(b) shows the waveforms after carrier synchronization by the proposed method. The phase difference δ becomes approximately 0.37° (0.1 μs). The carrier phase difference is not 0° due to errors in the current phase calculation. This is due to quantization errors. The maximum error of the phase due to quantization error is 1/2 of the sampling period (2us). The phase difference after carrier synchronization is less than the maximum error of the phase due to quantization error. Thus, the proposed method achieves carrier synchronization. In addition, the RMS value of the AC component of the circulating current after carrier synchronization becoms 250 mA. The circulating current is suppressed to less than 66% of the rated current by carrier synchronization.

Fig. 10 shows the waveforms of the inductor current and circulating current near zero crossing of the grid voltage. The initial phase difference δ is set to 15°. The inductor current is not a triangular wave, and the current ripple is 4.4 A before carrier synchronization. Fig. 11(b) shows the waveforms after carrier synchronization by the proposed method. The inductor current after carrier synchronization is almost a triangular wave. In addition, the inductor current ripple is 4.1A. Therefore, the RMS value of the inductor current is also reduced by carrier synchronization.

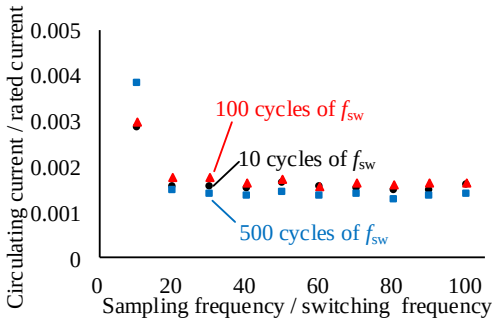

Fig. 8. Circulating currents versus sampling frequency and FFT calculation period. The circulating current is suppressed as the sampling frequency is larger and the FFT computation period is longer.

Table 2 Simulation condition.

Quantity	Symbol	Value
DC voltage	V_{DC}	200 V
Grid voltage	v_{ac}	100 V_{rms}
Grid frequency	f	50 Hz
Rated current of one unit	i_{ac}	10 A_{rms}
Rated power of one unit	P_1,P_2	1 kW
Grid side inductance	L_1	240 μH (%Z=3.6%)
Inverter side inductance	L_2	440 μH (%Z=2.8%)
Switching frequency	f_{sw}	10 kHz
Sampling frequency	f_{samp}	250 kHz
FFT calculation period		0.05 s

Conclusion

This paper proposed a carrier synchronized control of two inverters connected in parallel using high-speed sampling. In the proposed control, carrier synchronization is achieved by calculating the active power using fast sampling and adjusting the carrier phase to minimize the active power to zero. This control does not require information from the other inverters. Thus, the signal lines to the other inverter and the master

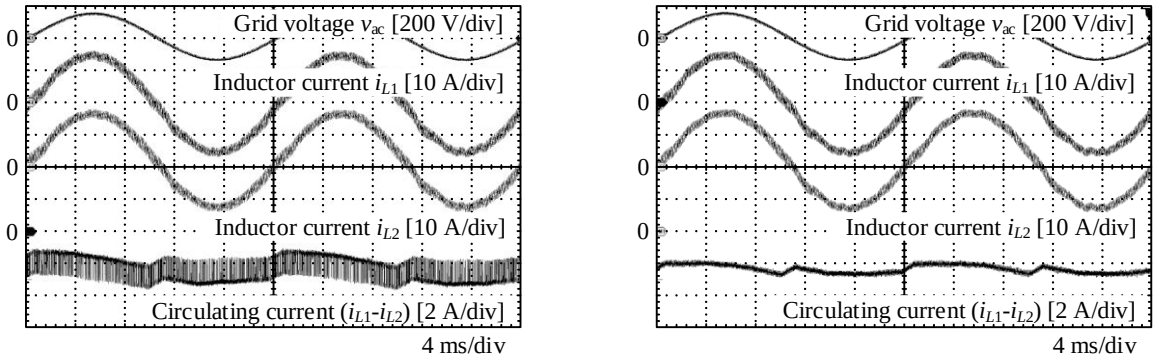

Fig. 9. The grid voltage, inductor currents, and circulating current. The circulating current is suppressed by carrier synchronization. (a) Before carrier synchronization. (b) After carrier synchronization.

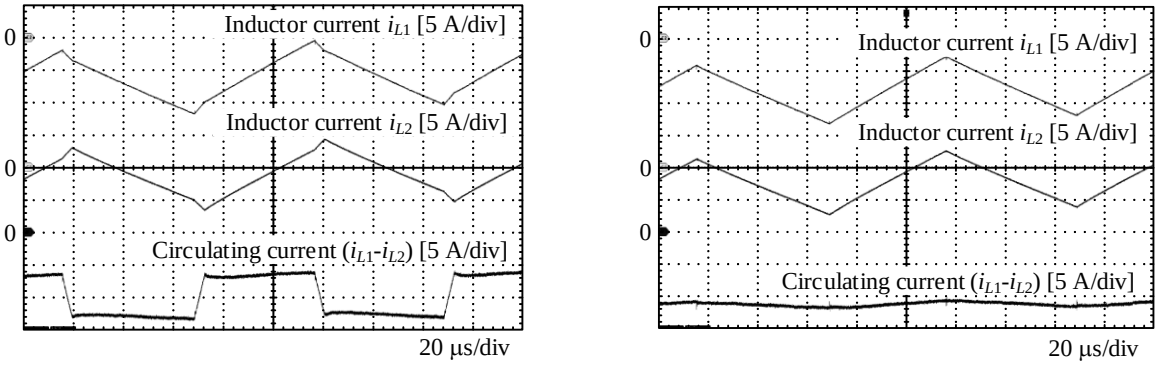

Fig. 10. Inductor currents and the circulating current near zero crossing of grid voltage. Inductor currents before carrier synchronization are not triangular, but after carrier synchronization they are almost triangular. (a) Before carrier synchronization. (b) After carrier synchronization.

controller are not required. In addition, the circulating current is suppressed by setting the sampling frequency and FFT period appropriately to suppress the effect of quantization errors. Experimental verification showed that the proposed method suppressed the circulating current to less than 66% of the rated current. These results verified the effectiveness of the proposed method. In the future, the proposed method will be verified under higher frequency conditions using the USPM controller.

References

[1]. Atsuo Kawamura, Yukinori Tsuruta and Hidemine Obara: Over 99.7% Efficiency at 100kW DC-DC Power Conversion using a 3.3kV SiC Device and Discussion on Device *dv/dt* Estimation, IEEJ Journal of Industry Applications, Vol. 13, No. 4, pp-426-436, 2024.

[2]. Parthasarathy Nayak, Kaushik Rajashekara and Sumit Kumar Pramanick: Soft-Switched Modulation Technique for a Single-Stage Matrix-Type Isolated DC–AC Converter, IEEE Transactions on Industry Applications, Vol. 55, No. 6, pp.7642-7656, 2019

[3]. Changjiang Sun, Xin Zhang, Jianwen Zhang, Miao Zhu and Jingjing Huang: Hybrid Input-Series–Output-Series Modular DC–DC Converter Constituted by Resonant and Nonresonant Dual Active Bridge Modules, IEEE Transactions on Industrial Electronics, Vol. 69, No. 1, pp.1062-1069, 2022.

[4]. Mingyao Ma, Xiangning He, Rongxiang Zhao and Dong Wang: Synchronization Analysis of Space-Vector PWM Converters With Distributed Control, IEEE Transactions on Power Electronics, Vol. 25, No. 12, pp.3026-3036, 2010.

[5]. Amrit R. Iyer, Rajendra Prasad Kandula, Rohit Moghe, Jorge E. Hernandez, Frank C. Lambert and Deepak Divan: Validation of the Plug-and-Play AC/AC Power Electronics Building Block (AC-PEBB) for Medium-Voltage Grid Control Applications, IEEE Transactions on

Industry Applications, Vol. 50, No. 5, pp.3549-3557, 2014.

[6]. Mana Sakamoto and Hitoshi Haga: Control Method for Universal Smart Power Module Considering Wireless Communication, IEEJ Journal of Industry Applications, Vol. 12, No.2, pp.204-214,2023.

[7]. Daiske Hiroe, Xiaohan Zhang, Kazuki Nakamura, Kotaro Sato, Ryosuke Suzuki, Kantaro Yoshimoto and Tomoki Yokoyama: A Study of 10MHz Multi-Sampling Deadbeat Control for PMSM Drive System using USPM Controller, IEEJ Journal of Industry Applications, Vol. 12, No. 3, pp. 508-516, 2023

[8]. K. Yamanokuchi, Hiroki Watanabe and Jun-ichi Itoh: Distributed Control Method for Power Conversion System With Series-Connected Autonomous Modular Converters, IEEE Transaction on Power Electronics, Vol. 38, No. 12, pp. 15242-15252, 2023

[9]. Max A. Parker, Li Ran and Stephen J. Finney: Distributed Control of a Fault-Tolerant Modular Multilevel Inverter for Direct-Drive Wind Turbine Grid Interfacing, IEEE Transactions on Industrial Electronics, Vol. 60, No. 2, pp. 509-522, 2013

[10]. Jian Hu and Hao Ma: Synchronization of the carrier wave of parallel three-phase inverters with virtual oscillator control, IEEE Transactions on power electronics, Vol. 32, No.10, pp.7998-8007, 2017

[11]. Tao Xu, Feng Gao, Xiongfei Wang and Frede Blaabjerg: A Carrier Synchronization Method for Global Synchronous Pulsewidth Modulation Application Using Phase-Locked Loop, IEEE Transactions on power electronics, Vol. 34, No. 11, pp.10720-10732, 2019

[12]. Kanta Suzuki, Kento Honda, Daisuke Hiroe and Tomoki Yokoyama: Basic Study on Instantaneous FFT Analysis Method of Power Electronics Equipment Using USPM Controller, 2024 IEEJ Industry Applications Society Conference, 1-30, pp. 163- 164, 2023